

HST observations, along with the ground-based results presented elsewhere in this issue<sup>14</sup>, show that the new generation of large telescopes should allow us to collect additional measurements that will be valuable in constraining the theories of ring-arc formation around Neptune. □

Received 18 March; accepted 6 July 1999.

- Hubbard, W. B. *et al.* Occultation detection of a neptunian ring-like arc. *Nature* **319**, 636–640 (1986).
- Lissauer, J. J. Shepherding model for Neptune's arc ring. *Nature* **318**, 544–545 (1985).
- Goldreich, P., Tremaine, S. & Borderies, N. Towards a theory for Neptune's arc rings. *Astron. J.* **92**, 490–494 (1986).
- Porco, C. C. An explanation for Neptune's ring arcs. *Science* **253**, 995–1001 (1991).
- Thompson, R. L., Rieke, M., Schneider, G., Hines, D. C. & Corbin, M. Initial on-orbit performance of NICMOS. *Astrophys. J.* **492**, L95–L97 (1998).
- Smith, B. A. *et al.* Voyager 2 at Neptune: Imaging science results. *Science* **246**, 1422–1449 (1989).
- Nicholson, P. D., Mosqueira, I. & Matthews, K. Stellar occultation observations of Neptune's rings. *Icarus* **113**, 295–330 (1995).
- Terrile, R. J. *et al.* First infrared imaging of the Neptune ring arcs: HST/NICMOS results. *Bull. Am. Astron. Soc.* **30**, 1044 (1998).
- Porco, C. C., Nicholson, P. D., Cuzzi, J. F., Lissauer, J. J. & Esposito, L. W. in *Neptune and Triton* (ed. Cruikshank, D. P.) 703–806 (Univ. Arizona Press, Tucson, 1985).
- Elliot, J. L. & Nicholson, P. D. in *Planetary Rings* (eds Greenberg, R. & Brahic, A.) 25–72 (Univ. Arizona Press, Tucson, 1984).
- Horany, M. & Porco, C. C. Where exactly are the arcs of Neptune? *Icarus* **106**, 525–535 (1993).
- Owen, W. M., Vaughan, R. M. & Synnott, S. P. Orbits of the six new satellites of Neptune. *Astron. J.* **101**, 1511–1515 (1991).
- Foryta, D. W. & Sicardy, B. The dynamics of the neptunian Adams ring's arcs. *Icarus* **123**, 129–167 (1996).
- Sicardy, B. *et al.* Images of Neptune's ring arcs obtained by a ground-based telescope. *Nature* **400**, 731–733 (1999).

**Acknowledgements.** We thank R. Thompson and M. Rieke from the NICMOS IDT team as well as P. Nicholson for calculating the predicted offsets of the arcs for 20 and 22 October 1998, and R. Jacobson for providing us with the coordinates of the normal of the orbital planes of the neptunian inner satellites.

Correspondence and requests for materials should be addressed to C.D. (e-mail: Christophe.Dumas@pl-nasa.gov).

## Linking insulator-to-metal transitions at zero and finite magnetic fields

Y. Hanein\*, N. Nenadovic\*, D. Shahar\*, Hadas Shtrikman\*, J. Yoon†, C. C. Li† & D. C. Tsui†

\* Department of Condensed Matter Physics, Weizmann Institute, Rehovot 76100, Israel

† Department of Electrical Engineering, Princeton University, Princeton, New Jersey 08544, USA

For many years, it was widely accepted<sup>1</sup> that electrons confined to two dimensions would adopt an insulating ground state at zero temperature and in zero magnetic field. Application of a strong perpendicular magnetic field changes this picture, resulting<sup>2,3</sup> in a transition from the insulating phase to a metallic quantum Hall state. Unexpectedly, an insulator-to-metal transition was recently observed<sup>4</sup> in high-quality two-dimensional systems at zero magnetic field on changing the charge carrier density. The mechanism underlying this transition remains unknown<sup>5–9</sup>. Here we investigate the magnetic-field-driven transition in a two-dimensional gallium arsenide system, which also exhibits<sup>10–12</sup> the poorly understood zero-field transition. We find that, on increasing the carrier density, the critical magnetic field needed to produce an insulator-to-metal transition decreases continuously and becomes zero at the carrier density appropriate to the zero-field transition. Our results suggest that both the finite- and zero-magnetic field transitions share a common physical origin.

In Fig. 1a we plot the resistivity ( $\rho$ ) of one of our samples as a function of magnetic field ( $B$ ) at several temperatures, with the density of holes ( $p$ ) held fixed. The sample is a p-type, inverted semiconductor–insulator–semiconductor (ISIS) sample<sup>13</sup> grown on the (311)A GaAs substrate<sup>14</sup> with silicon as a p-type dopant. At  $B = 0$  the system is insulating, as indicated by a rapidly increasing  $\rho$

as the temperature ( $T$ ) approaches zero. The insulating behaviour is maintained for  $B < B_c^L$ . For  $B > B_c^L$ , a quantum-Hall (QH) state ( $\nu = 1$ , where  $\nu$  is the Landau-level filling factor) is observed with  $\rho$  tending to zero as  $T$  is lowered. We identify  $B_c^L$ , the point where the temperature coefficient of resistivity (TCR) changes its sign, with the critical point of the insulator-to-QH transition<sup>2</sup>. At still higher  $B$ , beyond the  $\nu = 1$  QH state, the system turns insulating and a second  $T$ -independent transition point is seen at  $B_c^H$ .  $B_c^H$  therefore marks the critical  $B$  of the QH-to-insulator transition<sup>15</sup>. Following the path set by earlier studies<sup>10,16,17</sup> we focus, for now, on the low- $B$  transition and follow, in Fig. 1b–e, the evolution of the critical point  $B_c^L$  as we increase  $p$ .

Data obtained from the same sample at successive increases of the hole density are shown in Fig. 1b–e. Similarly to Fig. 1a, a low- $B$  transition point is evident in Fig. 1b, but occurs at a lower  $B$ . This trend continues in Fig. 1c until finally, in Fig. 1d, the crossing point disappears. In addition to the shift of  $B_c^L$  towards lower  $B$ , the higher  $p$  causes more QH states to become experimentally observable.

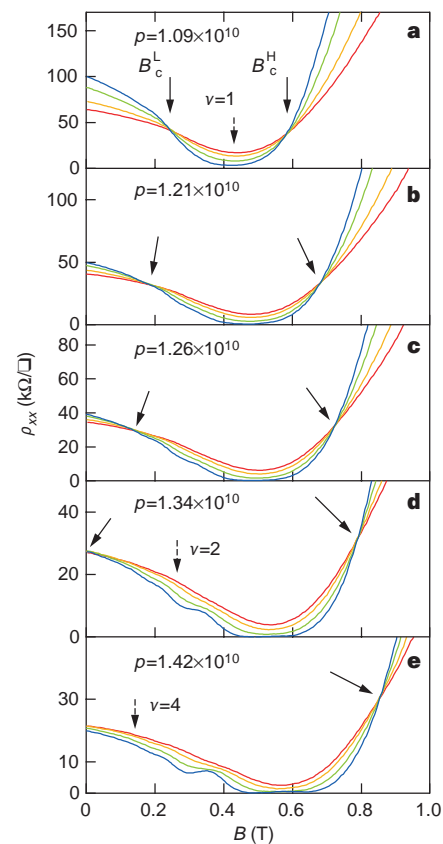


**Figure 1** Isotherms of the magnetoresistance data of sample H324Bc at various hole densities. In ISIS samples, the hole carrier-density ( $p$ ) is varied by applying voltage ( $V_g$ ) to the grown back-gate of the ISIS. The ohmic contacts to the two-dimensional layer have to be alloyed very carefully to avoid an electrical short between this layer and the underlying gate. As a result, the use of an ISIS structure is accompanied by complications in realizing reliable ohmic contacts at extremely low  $p$ s and low  $T$ s. In most of our devices, only some of the alloyed contacts survive at low  $T$  and low  $p$ . For the sample in this study, we do not have Hall measurements compatible with the set of measurements we present here. The sample was wet-etched to the shape of a standard ‘Hall bar’ (60 × 120  $\mu\text{m}$ ) and the measurements were done in a dilution refrigerator with a base  $T$  of 57 mK, using the a.c. lock-in technique with an excitation current of 1 nA flowing in the [01 $\bar{1}$ ] direction. The traces are colour coded with blue being low, and red being high, temperature: values of 63, 122, 177 and 217 mK were used at each  $p$  value. The solid arrows indicate the position of the crossing points, and the dashed arrows the position of the  $\nu = 1, 2$  and 4 filling factors. Resistivity along the current direction ( $\rho_{xx}$ ) was measured in units of  $k\Omega$  per square.

Hence the transition is no longer from an insulator to the  $\nu = 1$  QH state, but involves the  $\nu = 2$  (and higher, Fig. 1c) state. Eventually, the metallic behaviour at the high- $B$  side of the transition is too weak to be experimentally identified with a QH state.

Along with the shift in  $B_c^L$  and the evolution of the QH states, we notice in Fig. 1a–c that the insulating behaviour at  $B = 0$  becomes weaker until, in Fig. 1d,  $\rho$  at  $B = 0$  is  $T$ -independent. In Fig. 1e, the system has crossed over into its metallic phase and no low- $B$  transition, or  $T$ -independent point, is seen; this implies that the hole density shown in Fig. 1d ( $p = 1.34 \times 10^{10} \text{ cm}^{-2}$ ) is the critical density of the metal–insulator transition (MIT) at  $B = 0$ . This  $B = 0$  transition is the MIT in two dimensions first reported by Kravchenko *et al.* for Si samples<sup>4</sup>. Our main result can now be stated: on increasing  $p$ ,  $B_c^L$  gradually tends to lower  $B$ s, eventually converging to the  $B = 0$  MIT which, for this sample, takes place at  $p = 1.34 \times 10^{10} \text{ cm}^{-2}$ .

To complement our  $p$ -dependence study of the  $B$ -driven transitions, we next focus on the effect of a perpendicular magnetic field on the  $p$ -driven transition. Our new starting point is the more conventional experimental demonstration of the  $B = 0$  MIT in two dimensions. In Fig. 2a we plot  $\rho$  as a function of  $p$  at several  $T$ s and at  $B = 0$ . A  $T$ -independent crossing point is seen here as well (at  $p_c = 1.34 \times 10^{10} \text{ cm}^{-2}$ ), marking the transition from insulating behaviour for  $p < p_c$  to metallic behaviour for  $p > p_c$ . We then repeat the measurement of Fig. 2a at different values of  $B$  (Fig. 2b–e). In Fig. 2b and c,  $p_c$  shifts to a lower value, a trend which reverses for  $B > 0.35$  T (Fig. 2d and e). This trend reversal of  $p_c(B)$  is accompanied by the development of non-monotonic dependence of

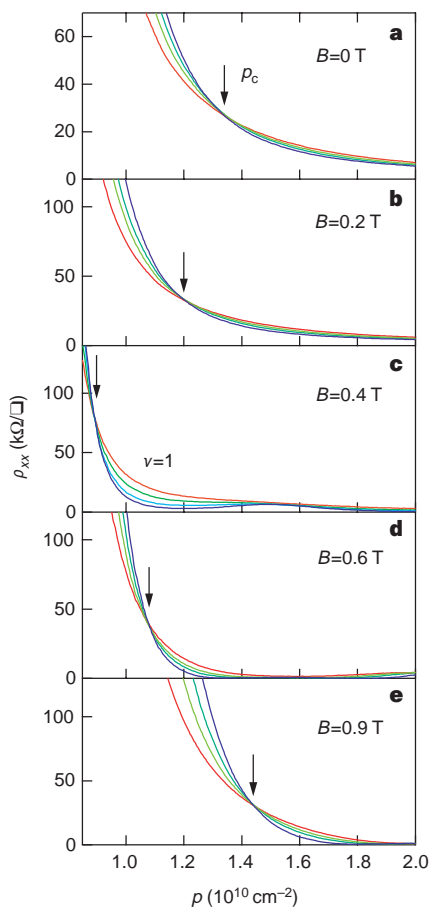


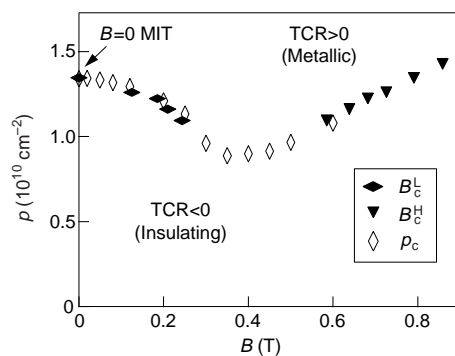
**Figure 2** Isotherms of the resistance versus  $p$  of sample H324Bc at various magnetic fields. The traces are colour coded with blue being low  $T$ , and red being high  $T$ . **a**,  $B = 0$  T at  $T = 57, 120, 160$  and  $214$  mK. **b**,  $B = 0.2$  T at  $T = 58, 121, 160$  and  $217$  mK. **c**,  $B = 0.4$  T at  $T = 60, 98, 148$  and  $212$  mK. **d**,  $B = 0.6$  T at  $T = 59, 122, 161$  and  $217$  mK. **e**,  $B = 0.9$  T at  $T = 59, 122, 161$  and  $217$  mK.

$\rho$  on  $p$ , which is a precursor to the QH effect. We now combine these  $p_c(B)$  results with the  $B_c(p)$  of Fig. 1, to plot a comprehensive phase diagram of our system in the  $B$ – $p$  plane.

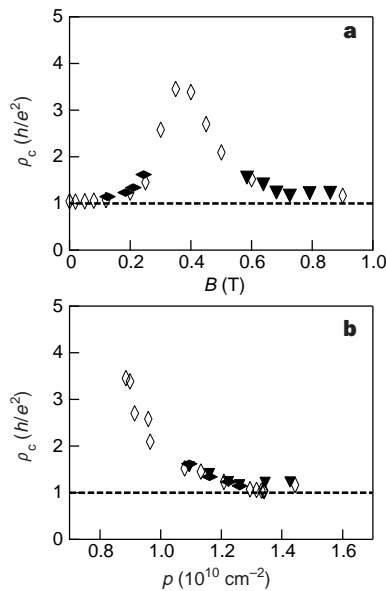
The phase diagram obtained from our data is shown in Fig. 3, where we plot the  $B$  and  $p$  coordinates of each of the transitions. Separate symbols are given to  $B_c^L$  and  $B_c^H$ , defined in Fig. 1, and to  $p_c$  from Fig. 2. Several points emerge from inspecting the resulting phase diagram. First, we note that the results obtained from the two data sets (fixed  $p$  and fixed  $B$  measurements) are mutually consistent. Second, for fixed  $p$ s in the range  $(0.88\text{--}1.33) \times 10^{10} \text{ cm}^{-2}$ , the low- $B$  insulating phase first turns metallic and then reappears at high  $B$ . This re-entrant nature of the insulating phase is clearly reflected in the  $B$  traces of Fig. 1a–c. And third, the low- $B$  region of the phase boundary reiterates the main result of our work and clearly depicts the continuous evolution of the transition from the high- $B$  MIT to the  $B = 0$  MIT. The relation between the transition at finite  $B$  and the MIT transition at  $B = 0$  suggests that similar processes govern the transport for both transitions<sup>18</sup>.

Figure 3 also includes the high- $B$  side of the phase diagram ( $B_c^H$ ). In fact, the low- and high- $B$  regimes are smoothly connected to form a single phase-boundary line. It is common practice to describe the finite- $B$  transitions in the language of quantum phase transitions<sup>19</sup>. If we assume that the phase-boundary line of Fig. 3 comprises a set of quantum critical points, it is possible that universal features should be observed in its vicinity. To test this proposition we examine the value of  $\rho$  at the transition points,  $\rho_c$ . In Fig. 4a we plot  $\rho_c$  of our transitions as a function of  $B$ . Overall,  $\rho_c$  is not constant, its value changing by almost a factor of 4 over our  $B$  range. However, at very low as well as at very high  $B$ ,  $\rho_c$  approaches a value close to  $h/e^2$ , the quantum unit of resistance. Although for our sample, at  $B = 0$ ,  $\rho_c$  is close to  $h/e^2$ , we point out that the value of  $\rho_c$  at  $B = 0$  obtained for other samples varies by an order of magnitude, between  $0.4h/e^2$  and  $4h/e^2$  (ref. 20).

Because of the clear separation of the  $B$ – $p$  plane into conducting and non-conducting regions, it is tempting to consider them as two unique phases for the entire  $B$  range. However, the nature of these phases may not be the same for all  $B$  values. Considering the metallic phase: at very low  $p$ , the metallic-like behaviour is due to the formation of the  $\nu = 1$  QH state. At higher  $p$ s, the metallic side of the transition appears to be due to a higher-order QH state, with  $\nu = 2$  or 4. However,  $\rho$  in these higher-order states does not vanish, and a clear determination of the nature of the metallic conduction is uncertain. In fact, due to the higher disorder at low  $p$ , a fully developed QH state is not expected at any experimentally reasonable  $T$ . The proximity to a MIT point is also a contributing factor to the ambiguity in determining the properties of the metallic region. Our data therefore preclude us from ruling out the possibility of the existence of an additional transition separating the metallic phase at



**Figure 3**  $B$  and  $p$  coordinates of the crossing points. The latter are derived from data similar to those of Figs 1a–e and 2a–e. Open diamonds denote  $p_c$ , filled diamonds denote  $B_c^L$  and filled triangles denote  $B_c^H$ . The arrow points to the  $B = 0$  metal–insulator transition (MIT). TCR is the temperature coefficient of resistivity.



**Figure 4** The value of  $\rho_c$  at the crossing points. The latter are derived from data similar to those of Figs 1a–f and 2a–e. **a**,  $\rho_c$  plotted as a function of  $B$ . Open diamonds denote  $\rho_c$  from  $p_c$  data, filled diamonds denote  $B_c^L$  data and filled triangles denote  $B_c^H$  data. **b**,  $\rho_c$  plotted as a function of  $p$ ; symbols as **a**.

low  $B$  and the QH phase at higher  $B$ . We note that experimental data<sup>21,22</sup> suggest that in the limit of zero temperature a metallic phase does not exist at any finite  $B$ . Hence, the nature of the metallic behaviour for the entire  $B$  range remains open for future investigation.

We have shown that  $B_c^L$ ,  $B_c^H$  and  $p_c$  define a common phase-boundary line in the  $B$ – $p$  plane, and that at intermediate  $B$ s along this phase boundary  $\rho_c$  significantly deviates from  $h/e^2$ , its value near  $B = 0$  and at high  $B$ . It is instructive to consider the dependence of  $\rho_c$  on  $p$ , rather than on  $B$ . In Fig. 1a–c we can readily see the general trend: the  $\rho_c$  of the low- $B$  and high- $B$  transitions at fixed  $p$  are very close to each other. To test this result for our entire range of  $p$  we plot, in Fig. 4b,  $\rho_c$  versus  $p$  obtained from our data. The two transitions are seen to have collapsed onto a single curve for our entire range of  $p$ , indicating that, for a given carrier density, the  $\rho_c$  of the low- $B$  and the high- $B$  transitions is the same. This supports the notion of symmetry between these transitions<sup>23</sup>.

A possible relation between different transitions in two-dimensional systems was noted by Jiang *et al.*<sup>2</sup>, who pointed out the similarities between the insulator-to-QH state and the insulator-to-superconductor transitions; the theoretical basis for such similarity has been reported<sup>3,18,24,25</sup>. In our work we found a relation between the finite- $B$  conductivity transitions and the metal–insulator transition at  $B = 0$ . As all transitions are measured in the same two-dimensional system, we were able to continuously transform one to the other. This raises the possibility that both transitions share a common physical origin. □

Received 22 January; accepted 17 June 1999.

1. Abrahams, E., Anderson, P. W., Licciardello, D. C. & Ramakrishnan, T. V. Scaling theory of localization: Absence of quantum diffusion in two dimensions. *Phys. Rev. Lett.* **42**, 673–676 (1979).
2. Jiang, H. W., Johnson, C. E., Wang, K. L. & Hannahs, S. T. Observation of magnetic-field-induced delocalization-transition from Anderson insulator to quantum Hall conductor. *Phys. Rev. Lett.* **71**, 1439–1442 (1993).
3. Kivelson, S., Lee, D. H. & Zhang, S. C. Global phase diagram in the quantum Hall effect. *Phys. Rev. B* **46**, 2223–2238 (1992).
4. Kravchenko, S. V., Kravchenko, G. V., Furneaux, J. E., Pudalov, V. M. & D'Iorio, M. Possible metal-insulator transition at  $B = 0$  in two dimensions. *Phys. Rev. B* **50**, 8039–8042 (1994).
5. Finkelstein, A. M. Influence of Coulomb interaction on the properties of disordered metals. *JETP* **57**, 97–108 (1983).
6. Dobrosavljevic, V., Abrahams, E., Miranda, E. & Chakravarty, S. Scaling theory of two-dimensional metal-insulator transitions. *Phys. Rev. Lett.* **79**, 455–458 (1997).
7. Altshuler, B. L. & Maslov, D. L. Theory of metal-insulator transitions in gated semiconductors. *Phys. Rev. Lett.* **82**, 145–148 (1999).

8. Phillips, P., Wan, Y. L., Martin, I., Knysch, S. & Dalidovich, D. Superconductivity in a two-dimensional electron gas. *Nature* **395**, 253–257 (1998).
9. He, S. & Xie, X. C. New liquid phase and metal-insulator transition in Si-MOSFETs. *Phys. Rev. Lett.* **80**, 3324–3327 (1998).
10. Simmons, M. Y. *et al.* Metal-insulator transition at  $B = 0$  in an ultra-low density two dimensional hole gas. *Physica B* **251**, 705–709 (1998).
11. Simmons, M. Y. *et al.* Metal-insulator transition at  $B = 0$  in a dilute two dimensional GaAs-AlGaAs hole gas. *Phys. Rev. Lett.* **80**, 1292–1295 (1998).
12. Hanein, Y. *et al.* The metalliclike conductivity of a two-dimensional hole system. *Phys. Rev. Lett.* **80**, 1288–1291 (1998).
13. Meirav, U., Heiblum, M. & Stern, F. High-mobility variable-density two-dimensional electron gas in inverted GaAs-AlGaAs heterojunctions. *Appl. Phys. Lett.* **52**, 1268–1270 (1988).
14. Hanein, Y., Shtrikman, H. & Meirav, U. Very low density two-dimensional hole gas in an inverted GaAs/AlAs interface. *Appl. Phys. Lett.* **70**, 1426–1428 (1997).
15. Shahaar, D., Tsui, D. C., Shayegan, M., Bhatt, R. N. & Cunningham, J. E. Universal conductivity at the quantum Hall liquid to insulator transition. *Phys. Rev. Lett.* **74**, 4511–4514 (1995).
16. Shashkin, A. A., Dolgoplov, V. T. & Kravchenko, G. V. Insulating phases in a two-dimensional electron system of high mobility Si MOSFET's. *Phys. Rev. B* **49**, 14486–14495 (1994).
17. Dultz, S. C., Jiang, H. W. & Schaff, W. J. Absence of floating delocalization states in a two-dimensional hole gas. *Phys. Rev. B* **58**, R7532–R7535 (1998).
18. Shimshoni, E., Auerbach, A. & Kapitulnik, A. Transport through quantum melts. *Phys. Rev. Lett.* **80**, 3352–3355 (1998).
19. Sondhi, S. L., Girvin, S. M., Carini, J. P. & Shahaar, D. Continuous quantum phase transitions. *Rev. Mod. Phys.* **69**, 315–333 (1997).
20. Hanein, Y., Shahaar, D., Yoon, J., Li, C. C., Tsui, D. C. & Shtrikman, H. Observation of the metal-insulator transition in two-dimensional n-type GaAs. *Phys. Rev. B* **58**, R13338–R13340 (1998).
21. Simonian, D., Kravchenko, S. V., Sarachik, M. P. & Pudalov, V. M. Magnetic field suppression of the conducting phase in two dimensions. *Phys. Rev. Lett.* **79**, 2340–2307 (1997).
22. Pudalov, V. M., Bruthaler, G., Prinz, A. & Bauer, G. Instability of the two-dimensional metallic phase to a parallel magnetic field. *JETP Lett.* **65**, 932–937 (1997).
23. Hilke, M. *et al.* Symmetry in the insulator-Hall-insulator transitions observed in a Ge/SiGe quantum well. *Phys. Rev. B* **56**, 15545–15548 (1997).
24. Fisher, M. P. A. & Lee, D. H. Anyon superconductivity and the fractional quantum Hall effect. *Phys. Rev. Lett.* **63**, 903–906 (1989).
25. Fisher, M. P. A., Grinstein, G. & Girvin, S. M. Presence of quantum diffusion in two dimensions: Universal resistance at the superconductor-insulator transition. *Phys. Rev. Lett.* **64**, 587–590 (1990).

**Acknowledgements.** We thank E. Shinshoni, M. Hilke and A. Yacoby for discussions. This work was supported by the NSF, the US-Israel BSF and by the Israeli Ministry of Science and the Arts.

Correspondence and requests for materials should be addressed to Y.H. (e-mail: hanin@wis.weizmann.ac.il).

## Observation of short-range critical wetting

D. Ross, D. Bonn & J. Meunier

Laboratoire de Physique Statistique de l'ENS, UMR 8550 du CNRS, associé aux universités Paris VI et Paris VII 24 rue Lhomond, 75231 Paris cedex 05, France

Mean-field theory correctly predicts the critical behaviour of systems close to a phase transition, provided that fluctuations can be neglected. Fluctuations, however, become important if the dimensionality of the system is lower than a certain upper critical dimension. For such systems, it is necessary to use renormalization-group methods to describe the critical behaviour. Investigation of three-dimensional systems in which the upper critical dimension is also three can therefore provide a probe of the way in which mean-field theory breaks down when fluctuations become important<sup>1–12</sup>. An important example is the critical wetting transition that is predicted<sup>1,2</sup> to occur in systems in which long-range forces are negligible, involving a continuous and reversible increase in the thickness of an adsorbed film. Here we present experimental observations of the short-range wetting transition close to the critical point in methanol–alkane binary liquid mixtures. We observe second-order, critical wetting for nonane (as characterized by the surface specific-heat exponent). The measured value is consistent with the predictions of mean-field theory, but disagrees strongly with renormalization-group calculations, which predict<sup>1–4</sup> non-universal behaviour for this transition. The reasons for the apparent failure of the renormalization-group approach remain unclear; further experiments are needed to investigate the effects of fluctuations in more detail.

When a liquid droplet is put onto a surface, three different